NANO LETTERS

pubs.acs.org/NanoLett

Controlling Plasmonic Wave Packets in Silver Nanowires

Lina Cao,[†,‡] Rene A. Nome,[†,§] Jason M. Montgomery,[‡,∥] Stephen K. Gray,*[,‡] and Norbert F. Scherer*[,†,‡]

[†]Department of Chemistry and The James Franck Institute, 929 East 57th Street, The University of Chicago, Chicago, Illinois 60637 and [‡]Center for Nanoscale Materials, Argonne National Laboratory, Argonne, Illinois 60439

ABSTRACT Three-dimensional finite-difference time-domain simulations were performed to explore the excitation of surface plasmon resonances in long silver (Ag) nanowires. In particular, we show that it is possible to generate plasmonic wave packets that can propagate along the nanowire by exciting superpositions of surface plasmon resonances. By using an appropriately chirped pulse, it is possible to transiently achieve localization of the excitation at the distal end of the nanowire. Such designed coherent superpositions will allow realizing spatiotemporal control of plasmonic excitations for enhancing nonlinear responses in plasmonic "circuits".

KEYWORDS Nanophotonics, surface plasmons, nanowires, wave packet, control

Metallic nanostructures that support surface plasmons (SPs), collective electronic excitations near a metal/dielectric interface that manifest themselves as intense, evanescent electromagnetic surface waves, provide a promising route to create subwavelength photonic elements for optoelectronic devices and other applications.[1] For example, nanostructures for sensing that utilize linear electromagnetic interactions with SPs are emerging.[2] SPs are also especially intriguing in the context of nonlinear optical responses, such as in surface-enhanced Raman spectroscopy (SERS), owing to the huge electromagnetic field enhancements that are possible.[3]

Being able to develop controllable, high-intensity SP pulses and (transient) hot spots in nanostructures would thus be very desirable.[4,5] In this paper, we start to address this challenge for the case of SP excitations in long Ag nanowires. High-aspect ratio (e.g., 1:100 *w*/*l*) nanowires have been shown experimentally to sustain a series of specific SP resonances,[6] with features characteristic of Fabry-Pérot resonators.[7] These resonances or modes have wavelengths considerably shorter than the wavelength of the exciting light, and owing to the nonradiating character of the modes (aside from scattering at the nanowire ends), have large propagation lengths. Finite-difference time-domain (FDTD) calculations have reproduced the essential features of these experimental observations, further affirming that Ag nanowires are efficient "resonators".[3,8] Recent applications that utilize the long propagation length of plasmons in metallic nanowires include SERS[9] and plasmon-induced photon emission from quantum dots near the nanowires.[10]

Theoretical work has already indicated that tailored, ultrafast optical pulses have the ability to control the spatiotemporal dynamics of SPs in idealized metallic nanostructures[11,12] and in arrays of metallic cylinder structures.[13] Furthermore, recent experimental work[4] demonstrated the utility of control techniques such as chirping and phase modification for localization of the SP field enhancement. However, these studies did not explicitly address the superposition of SPs, to create "plasmonic wave packets" that are analogous to quantum mechanical ones.

In this Letter, we present the results of realistic, 3D FDTD simulations and analysis showing that it is indeed possible to create plasmonic "wave packets" as coherent superposition states of the plasmonic modes of realistic nanowire systems. The packet propagates with low loss and by applying an appropriate frequency-dependent phase to the electromagnetic pulsed used for excitation one can also temporally focus the wavepacket at particular positions along the wire. The coherence thus imparted to a multiresonance system is in direct analogy with wave packets and coherent control in molecular systems. We believe this represents an exciting step toward SP-based energy and information transport.

Figure 1, top panel, shows the Ag nanowire system studied here, which consists of an $L = 3$ μm long silver nanowire with diameter $d = 90$ nm whose surrounding medium is vacuum. The nanowire is treated as a simple, solid cylinder of Ag with both ends rounded into hemispheres. (The rounding of the ends is not essential; similar results are obtained with flat ends.) Our FDTD calculations were carried out using standard techniques.[15,16] The frequency (ω) dispersive and complex dielectric function for

* To whom correspondence should be addressed. E-mail: (S.K.G.) gray@anl.gov; (N.F.S.) nfschere@uchicago.edu.

[§] Institute of Chemistry, State University of Campinas, Campinas, SP, Brazil, 13083-970.

[∥] Department of Chemistry and Physics, Florida Southern College, Lakeland, FL 33801.

Received for review: 4/12/2010
Published on Web: 08/12/2010

DOI: 10.1021/nl101285t | *Nano Lett.* **2010,** *10,* 3389–3394

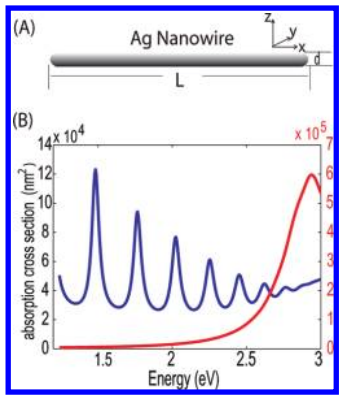

FIGURE 1. (A) Illustration of the system geometry. (B) Absorption spectrum for 3D nanowire ($L = 3\ \mu$m, $d = 90$ nm) with x-polarized (blue curve) and y-polarized (red curve) incident light. The incident light is a pulse with central frequency corresponding to 2.48 eV and duration ≈10 fs, which covers the spectrum range 1−3.5 eV and propagates along $+z$ axis.

Ag, $\varepsilon_{Ag}(\omega)$, was taken to be the Drude−Lorentzian model of ref 17, while the medium is vacuum. The model for $\varepsilon_{Ag}(\omega)$ is a fit to experimental data[18] and is implemented in the FDTD method with auxiliary differential equations.[15,16] Optical spectra are computed via propagation of an appropriate, finite (≈10 fs) duration plane wave and analysis of the flux through a box enclosing the nanowire. We carry out propagations until the field amplitudes have all decayed to $\sim 10^{-5}$ of the highest intensity in the FDTD box surrounding the nanowire, which occurs in 100−200 fs. See the Supporting Information for additional details of the simulation and parameters.

The lower panel of Figure 1 shows absorption spectra for x-polarized light incident from the negative z-axis direction and y-polarized light incident from the negative x-axis direction. The spectrum for light polarized along the longitudinal x-axis (blue curve) shows a series of absorption resonance peaks for various incident photon energies, $\hbar\omega$. These peaks can be associated with the simple resonance condition that a positive integer multiple, m, of SP half wavelengths, $\lambda_{SP}(\omega)/2$, equals the length L of the rod, hence

$$\lambda_{SP}(\omega) = \frac{2L}{m} \tag{1}$$

The positions of the resonances may be found by specifying the SP dispersion relation, $\lambda_{SP}(\omega)$ and solving eq 1 for ω. These resonances correspond to the Fabry-Pérot SP resonator states of ref 6. (Note that the decreasing peak intensities with increasing energy evident in Figure 1 is also consistent with the decrease in SP quality factor, $\mathrm{Re}(\varepsilon_{Ag})/\mathrm{Im}(\varepsilon_{Ag})$, as energy increases.)

There is a simple analogy of the Fabry-Pérot SP resonator states with quantum mechanical (QM) states that we would like to emphasize. Consider a particle of mass μ in a box of length L. The QM particle-in-a-box energy levels are $E = h^2n^2/(8\ \mu L^2)$, $n = 1, 2$, and so forth. These levels can be thought of as arising from the same argument as above by requiring $\lambda_{QM}(E) = 2L/n$ and then using the de Broglie dispersion relation $\lambda_{QM}(E) = h/(2\mu E)^{1/2}$ to solve for E. So, the difference lies in the dispersion relation employed. We can rewrite the QM dispersion in terms of wave vector as $k_{QM}(E) = 2\pi/\lambda_{QM}(E) = 2\pi\ (2\mu E)^{1/2}/h$. Light in vacuum, on the other hand, has dispersion $k(\omega) = \omega/c$ and is linear in the frequency or photon energy. The SP dispersion is different from that of ordinary light (see below) but is still approximately linear in the spectral region of interest. The different QM and SP dispersion relations account for the differences in the energetic spacings of adjacent levels as m or n increases; in the SP case (Figure 1), the spacings are nearly the same (or the ratio of energy differences is nearly constant), whereas in the particle-in-a-box case the spacings increase linearly with the quantum number. This simple analogy with quantum mechanics was the original motivation for studying SP wave packets in the Ag nanowire systems as we do here. It will also be helpful in the interpretation of our results.

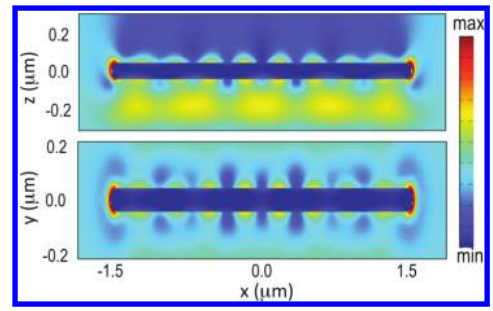

FIGURE 2. $|E|^2$ distribution (logarithmic scale) corresponding to $\hbar\omega = 1.49$ eV for a 3 μm × 90 nm Ag nanowire. Top panel is for the xz-plane at $y = 0$ while bottom panel is for the xy-plane at $z = 0$. Since the plane wave travels from $-z$ to $+z$, it leads to a shadow above and a reflected wave below the particle in the upper panel image.

A simple approximation to λ_{SP} is given by $\lambda_{SP} \approx \lambda_{SPP} \equiv 2\pi/k_{SPP}$, where k_{SPP} is the magnitude of the wave vector for surface plasmon polariton (SPP) propagation on a metal film/air interface[1]

$$k_{SPP}(\omega) = \frac{\omega}{c}\mathrm{Re}\left[\frac{\varepsilon_{Ag}(\omega)}{\varepsilon_{Ag}(\omega) + 1}\right]^{1/2} \tag{2}$$

In the present case of 3D nanowires, however, λ_{SPP} tends to be 20% larger than the actual λ_{SP} values that we infer from our full 3D calculations, a result that is consistent with experiment.[6] (See Supporting Information for a more detailed discussion, including comparison with finite-length 2D slabs in which case λ_{SPP} is an excellent approximation to λ_{SP}, as well as an analysis of the effect of the nanowire cross section diameter, d.)

Figure 2 displays the result of Fourier transforming the FDTD electric field at one specific resonance frequency, 1.49

DOI: 10.1021/nl101285t | Nano Lett. 2010, 10, 3389–3394

eV ($\lambda_{inc} = 832$ nm), showing the xy-plane (bottom) and xz-plane (top), respectively. The top panel of Figure 2 shows the interference of reflected and incident waves. The result in the bottom panel is less obscured by reflected waves, and one can count $m = 8$ half wavelengths. Notice also the very weak coupling to the far field as is evident by the low (dark blue) intensity above the rods (i.e., along z) except in the vicinity of the rod ends. Scattering at the ends is responsible for the coupling of light into and out of the modes.

Further calculations and analysis analogous to that described in the previous paragraph lead to the conclusion that all the absorption peaks in Figure 1 correspond to only $m =$ even mode numbers. Borrowing again from quantum mechanics, this "selection rule" is a result of symmetry. The system has reflection symmetry about the midpoint along x and the particular plane wave initial condition used has x-polarization so that E_x and H_y are symmetric with respect to reflection through the yz plane at the midpoint along x. These symmetries imply that E_z, the dominant electric field component of the resonances, must be antisymmetric with respect to reflection, thus forcing a node at the midpoint. More explicitly, if H_y is symmetric with respect to $x \rightarrow -x$, its derivative, $\partial H_y/\partial x$, is antisymmetric. This latter term occurs in the Maxwell equation for $\partial E_z/\partial t$ and so forces E_z to be antisymmetric. This "selection rule" then excludes the possibility of $m =$ odd states for the symmetrical excitation field (i.e., the extended plane wave).

We now turn to a less symmetric source to generate (excite) all the relevant resonances. One could use, for example, a Gaussian light beam focused on one end of the nanowire as in refs 3, 6, and 8. However, a simpler choice that should lead to similar results is a pulsed, soft dipole source that mimics the effect of emitters such as fluorescing quantum dots or molecules.[19,20] At each time step, in addition to the usual FDTD field updates, the longitudinal electric field component, E_x, is augmented by $f(t)$,[12] at a single point (one FDTD cubical grid point) near one end of the rod

$$f(t) = A(t)\sin[\omega_0 t + \varphi(t)] \tag{3}$$

where $A(t)$ is an envelope function chosen such that the pulse is on from the start of the simulation at time $t = -\tau$ to $+\tau$, ω_0 is the central frequency, and $\varphi(t)$ is a modulating phase, which can be used to create a chirped pulse. By choosing $\varphi(t) = \omega_0 \alpha t^2/\tau$, the effective frequency of the source is a function of time, $\omega_{eff}(t) = \omega_0(1 + \alpha t/\tau)$ with $\alpha > 0$ being a positive chirp (increasing frequency) and $\alpha < 0$ being a negative chirp (decreasing frequency).[12] A Blackman-Harris window function is used to define $A(t)$,[12] although a Gaussian function could also be used and yields similar results (the time-domain full width at half-maximum is approximately τ).

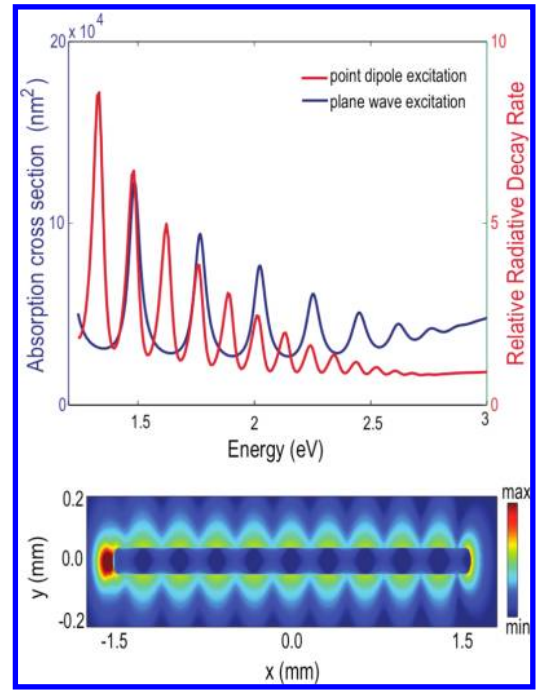

FIGURE 3. Top panel: absorption spectrum (blue curve) for plane wave excitation and relative radiative decay rate (Γ_r/Γ_0) for point dipole excitation for a 3 μm × 90 nm Ag nanowire. Bottom panel: time-averaged $|E|^2$ distribution (logarithmic scale) for a CW point dipole source at 1.62 eV.

The source is placed 40 nm from the center of the left-side edge of the rod. We first consider the case of no chirp, $\alpha = 0$, $\hbar\omega_0 = 2.48$ eV, and a pulse short enough, $2\tau \approx 10$ fs, to generate a signal with energy content in the 1.0−3.5 eV range, and energy domain full width at half-maximum $\hbar\Gamma \approx 0.75$ eV (see Supporting Information for additional details). The upper panel of Figure 3 shows (red curve) Γ_r/Γ_0, the ratio of the radiative decay rate of the dipole in the presence of the nanowire (Γ_r) and in its absence (Γ_0), which is inferred using the flux integral approach of ref 19. This result is very similar to the scattering spectra[3,6,8] obtained with focused Gaussian beams and, unlike the case of plane wave excitation (also shown as a blue curve), displays both even and odd m resonances. The lower panel shows a representative field profile of one of the odd m resonances obtained by time averaging with a continuous wave dipole source emitting at $E = 1.62$ eV ($\lambda = 764$ nm). The mode in Figure 3 has an x−y profile that is similar in appearance to the plane wave generated even mode of Figure 2. Its x−z profile (not shown), however, does not display a reflected wave.

It is important to note that because the spectrum in Figure 3 is obtained from the single (site initiated) propagation and contains many strong peaks that correspond to the various modes, a linear superposition of SP resonances is being created by the pulse. This situation is, therefore, very similar in spirit to quantum mechanical wave packets that are superpositions of bound or resonance states.[21] Thus, the evolving electromagnetic field can be thought of as a "plasmonic wave packet."

DOI: 10.1021/nl101285t | *Nano Lett.* **2010,** *10,* 3389–3394

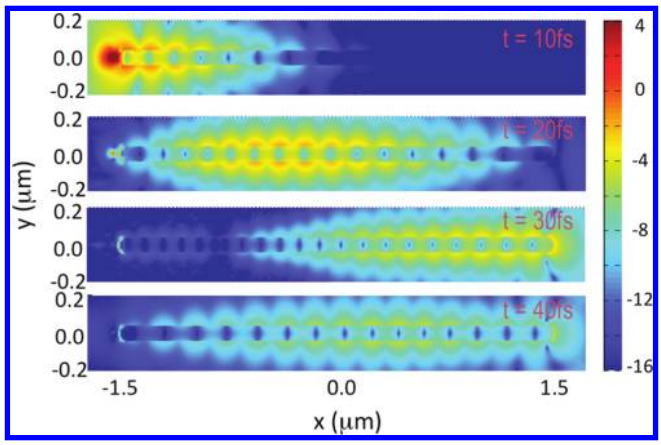

FIGURE 4. Electric field $|E|^2$ distribution (logarithmic scale) for pulsed point dipole excitation at different time steps. The central frequency of the initial pulse corresponds to 2.48 eV and its full width is $2\tau = 21$ fs.

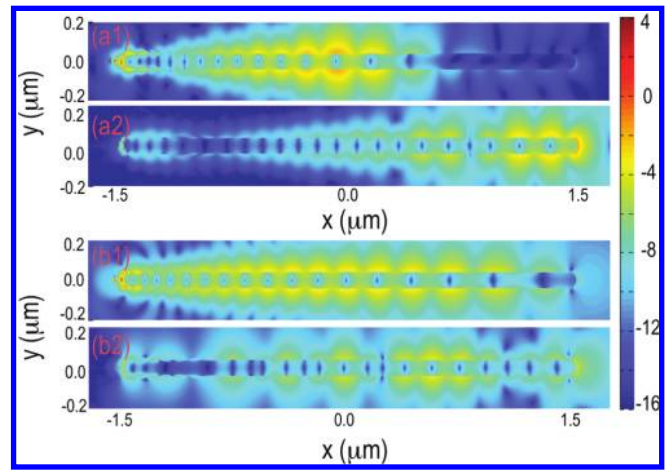

FIGURE 5. $|E|^2$ (logarithmic scale) for chirped pulse excitation at different times. For all the panels, the central frequency of the initial pulse corresponds to 2.48 eV with full width $2\tau = 21$ fs. Top two panels are for a negative chirp and bottom two panels are for a positive chirp. See text for more details. Panels a1 and b1 are for $t = 20$ fs and panels a2 and b2 are for $t = 30$ fs.

Snapshots of the evolving field intensities obtained when using the above unchirped pulse are shown in Figure 4. It is clear that there is indeed propagation along the wire. However, it is possible to achieve greater control over such propagation by introducing a modulation of the frequency-dependent phase or chirp. To motivate this idea, we note that $k_{SP} = 2\pi/\lambda_{SP} = m\pi/L$ from eq 1. The phase velocity associated with each mode is thus $v_p(m) = \omega(m)/k_{SP}(m)$, where $\omega(m)$ is the incident light frequency that excites mode m. From the observed resonance positions, we see that incident frequencies vary almost linearly with m: $\hbar\omega(m) \approx a_0 + a_1 m$ ($a_0 = 0.39$ eV and $a_1 = 0.14$ eV in our case). The phase velocity of each mode is thus

$$v_p(m) \approx \frac{a_1 L}{\hbar\pi} + \frac{a_0 L}{\hbar\pi}\left(\frac{1}{m}\right) \qquad (4)$$

that is, a decreasing function of m [or equivalently $\omega(m)$]. If one wished to obtain all modes in phase at the end of the rod at some time, it would make sense to first excite modes with smaller phase velocities and then at later times excite larger phase velocity modes. This suggests exciting high m or ω modes first and then the lower m or ω modes; that is, use a negatively chirped pulse.

The majority of our calculations presented in the subsequent figures use chirped pulses with $\hbar\omega_0 = 2.48$ eV, $2\tau = 21$ fs, $\alpha = \pm 0.63$, and a constant chirp rates of $\hbar d\omega_{eff}/dt = \pm 0.156$ eV/fs. Over the $t = -\tau$ to $+\tau$ period the pulse is on, ω_{eff} ranges from 0.92−4.07 eV ($\alpha > 0$) or 4.07−0.92 eV ($\alpha < 0$), with $\hbar\Gamma \approx 2.75$ eV. It should be noted that in typical experiments one starts with, ideally, a transform-limited unchirped pulse containing the spectral range of interest and passes it through appropriate materials to achieve a chirped pulse.[22] Present technology does not allow for generation of transform-limited pulses with such a large spectral range as used in most of our calculations, although less perfect (and thus more difficult to manipulate) ultrashort pulses can be prepared. However, experimentally one can achieve rod lengths, L, significantly longer than the 3 μm rods used in our calculations. Longer L leads to a much higher plasmon density of states (see eq 1), and thus reduces the required bandwidth and chirp rate. We will also report below on some calculations done with longer L values.

Figure 5 shows the resulting field intensity snapshots for the chirps discussed above. The two lower panels correspond to a positive chirp, while the upper pair of panels show the negative chirp result. It is evident that the negative chirp is leading to a more intense and focused plasmon wave packet at the distal end of the rod. For example, comparing the second panel in Figure 4 (no chirp, at $t = 20$ fs) with the corresponding panels a1 and b1 in Figure 5, we see that the wave packet width is narrowed by approximately a factor of 2 for the negatively chirped pulse and broadened by approximately by a factor of 2 for the positively chirped pulse. Furthermore, the highest field (i.e., peak) intensity along the wire shows a 2-fold enhancement in the negatively chirped case and a reduction of one-half for the positively chirped case compared to unchirped case.

Figure 6 quantifies the above points by plotting the electric field intensity as a function of time, at a point close to the distal end of the rod for the three chirps considered in Figures 4 and 5. In Figure 6, the negatively chirped result (red) is clearly much more focused and at least 2-fold greater peak intensity than the unchirped and positively chirped results. The inset of Figure 6 illustrates the pulse shapes for these calculations (Supporting Information Figure S4). A pulse with no chirp but with the same central frequency and frequency content as the chirped pulses in Figures 5 and 6 is also considered. The result is plotted as the black curve. Although this pulse does not produce any focusing, its

DOI: 10.1021/nl101285t | Nano Lett. 2010, 10, 3389–3394

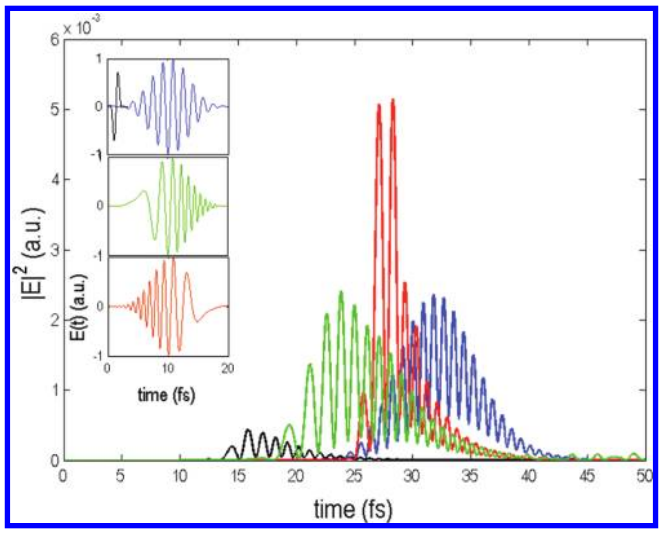

FIGURE 6. $|E|^2$ **(linear scale) near the distal end (**$x = L/2 + 40$ **nm,** $y = z = 0$**) of the nanowire for a positively chirped pulse (green curve), two no chirp pulses (blue and black curves), and a negatively chirped pulse (red curve). The inset shows the incident (exciting) pulse shapes. See text for greater detail.**

propagation does exemplify the temporal dispersion of the plasmonic wave packet in the rod.

The focusing result with the negative chirp in Figure 6 is very intriguing and represents a key result of this paper. We will now consider the two logical questions that arise concerning this result: (1) Can one further optimize the effect? and (2) Can such an effect be achieved in the laboratory?

A simple, intuitive argument for the focusing effect arises from the fact that the higher order modes propagate more slowly (eq 4). Thus, an excitation pulse that will cause focusing of the wave packet should excite the different modes at times coincident with the speed differences so that they all arrive at the distal end at the same time. However, there are issues that are either not important in the case of wave packet control in molecules or that transcend the analogy altogether. An analysis based on eq 4 (see Supporting Information) shows that ideal matching of the relative times of excitation would require an even larger chirp rate of $\hbar d\omega_{eff}/dt \sim -0.4$ eV/fs. This is not feasible when the pulse length (20 fs) is constrained and for frequency bandwidth used here. Simply lengthening the pulse duration can lead to the problematic "solution" that the pulse is longer than the time of propagation. That is, such a pulse is not "impulsive" on the time scale of the inverse mode spacing. This problem is typically not encountered in the case of controlling vibrational wavepackets in molecules since the anharmonicity is typically small compared to the vibrational level spacing so that chirp that needs to be imparted is small. Furthermore, higher order (i.e., beyond linear chirp) dispersion caused by the Ag nanowire is significant for the large spectral bandwidth used. Other factors, including mode coupling efficiencies must be considered. For example, we do not instantly excite each mode as the pulse frequency briefly passes through the relevant resonance frequency. It is likely that optimal coupling into the modes would be achieved with a lower chirp rate and this aspect counterbalances the simple arguments based on the dispersion relation

More complex pulse shapes based on optimal control theory ideas should be investigated.[21] One approach would be to begin with a desired final or optimal result and propagate it backward in time to obtain the requisite initial condition. While it may not be experimentally feasible to generate such an initial condition, some of its features could be incorporated into a more feasible one. It is interesting to note that Figure 6 effectively already contains an idea of such an optimal "initial condition." The black curve in the main panel is a 10 fs, positively chirped end result of propagating a 2 fs transform-limited, unchirped initial pulse (black curve in the inset). (See Supporting Information, Figure S7, for demonstration of the positive chirp character.) Microscopic reversibility can be used to suggest that an oppositely directed, negatively chirped version of the final result could serve as the initial condition to generate the highly localized result in the inset. Note that our calculations employ a pulsed dipole source and we are also ignoring the resulting forms for the other field components and so a fully optimized pulse, that is also experimentally feasible (see below) would require a variety of other calculations beyond the scope of the present paper.

In experiments, one can create a transform-limited unchirped pulse that contains the spectral range of interest and use appropriate optics (e.g., prisms, diffraction gratings) to achieve a chirped pulse.[22] Present technology does not allow generation of transform-limited pulses (2 fs) with the large spectral range used in most of our calculations. However, Ag wires of lengths, L, significantly longer than 3 μm are readily fabricated. Longer L leads to a much higher plasmon density of states (see eq 1), and thus reduces the required bandwidth and chirp rate. In this case, ≈10 fs duration pulses have sufficient bandwidth to create plasmonic superposition states and these pulses can readily be prepared in the laboratory. Furthermore, the Supporting Information (Figure S7) shows how such a pulse can be effectively chirped (in this case by the nanorod itself) to lead to an initial pulse capable of achieving the localization effect.

We have also carried out additional calculations to verify the experimental feasibility of achieving the above focusing effect. In the first set of calculations, a much lower chirp rate of 0.003 eV/fs and $2\tau \approx 60$ fs corresponding to a $\hbar\Gamma \approx 0.15$ eV. We examined rods of lengths $L = 3$, 6, and 10 μm long. The negative chirp still led to increasing focusing over the positive chirp, although the relative differences were small (5−15%). However, significantly, the focusing becomes stronger with increasing L. It is expected that longer rods ($L \approx 20$ μm) with $2\tau \approx 60$ fs can result in better focusing. A second type of calculation was to start with approximately the shortest experimentally achievable unchirped transform-limited pulse, $2\tau \approx 10$ fs ($\hbar\Gamma \approx 0.75$ eV), propagate it along an $L = 10$ μm nanowire, and Fourier analyze the resulting

DOI: 10.1021/nl101285t | *Nano Lett.* **2010,** *10,* 3389–3394

waveform at the end of the wire to obtain a spectrum in frequency (see Supporting Information). The result shows a positive chirp, implying that by using the corresponding negative chirp as the excitation source it should be possible to achieve focusing.

We have shown that it is possible to excite superpositions of SP resonance states in long silver nanorods (or nanowires) with a soft dipole excitation source at one end. These superpositions can propagate along the nanowire, that is, can be viewed as plasmonic wave packets. One of the most elementary forms of pulse-shaping, a linear chirp, when appropriately chosen, was shown to cause temporal focusing of the chirped wave packet at the far end of the nanorod. This finding is analogous to the "molecular canon" of Wilson and co-workers.[23]

The idea of dispersion compensation is ubiquitous in ultrafast optics and localizing plasmonic excitations has been suggested in theory and realized in experiment.[4] However, the resonance features that occur in Ag nanowires create clear analogies to coherent control in molecular spectroscopy. Furthermore, the temporal focusing of the plasmon will create high local fields and thus enhance nonlinear effects, for example, SHG,[24] or drive plasmon-enhanced photoemission to create electron pulses,[25] and may allow creating a true time-space resolved scanning probe instrument.[26,27] The resonances allow dense phase encoding of information for information transport that could have "simple" readouts at specific spatial locations or provide interesting and nontrivial reference fields in plasmonic interferometers. The realizations of some of these advances are underway in our current experiments.

Acknowledgment. We thank Dr. Matthew Pelton for many helpful discussions. We acknowledge financial support from the University of Chicago - Argonne National Laboratory Joint Theory Institute (JTI) program. Use of the Center for Nanoscale Materials was supported by the U. S. Department of Energy, Office of Science, Office of Basic Energy Sciences, under contract no. DE-AC02-06CH11357.

Supporting Information Available. Two and three dimensional nanowire results, detailed use of chirped pulses, the feasibility of optimization, and experimental feasibility, and additional figures. This material is available free of charge via the Internet at http://pubs.acs.org.

REFERENCES AND NOTES

(1) Barnes, W. L.; Dereux, A.; Ebbesen, T. W. *Nature* **2003**, *424*, 824–830.
(2) Stewart, M. E.; Anderton, C. R.; Thompson, L. B.; Maria, J.; Gray, S. K.; Rogers, J. A.; Nuzzo, R. G. *Chem. Rev.* **2008**, *108*, 494–521.
(3) Laroche, T.; Girard, C. *Appl. Phys. Lett.* **2006**, *89*, 233119.
(4) Aeschlimann, M.; Bauer, M.; Bayer, D.; Brixner, T.; et al. *Nature* **2007**, *446*, 301.
(5) Tuchscherer, T.; Rewitz, C.; Voronine1, D. V.; Garcia de Abajo, F. J.; Pfeiffer, W.; Brixner, T. *Opt. Express* **2009**, *17*, 14235.
(6) Ditlbacher, H.; Hohenau, A.; Wagner, D.; Kreibig, U.; Rogers, M.; Hofer, F.; Aussenegg, F. R.; Krenn, J. R. *Phys. Rev. Lett.* **2005**, *95*, 257403.
(7) Dorfmuller, J.; Vogelgesang, R.; Weitz, R. T.; Rockstuhl, C.; Etrich, C.; Pertsch, T.; Lederer, F.; Kern, K. *Nano Lett.* **2009**, *9*, 2372–2377.
(8) Laroche, T.; Vial, A.; Roussey, M. *Appl. Phys. Lett.* **2007**, *91*, 123101.
(9) J. A. Hutchison, J. A.; S. P. Centeno, S. P.; H. Odaka, H.; H. Fukumura, H.; J. Hofkens, J.; H. Uji-i, H. *Nano Lett.* **2009**, *9*, 995–1001.
(10) Wei, H.; Ratchford, D.; Li, X.; Xu, H.; Shih, C.-K. *Nano Lett.* **2009**, *9*, 4168–4171.
(11) Stockman, M. I.; Faleev, V.; Bergman, D. J. *Phys. Rev. Lett.* **2002**, *88*, No. 067402.
(12) Lee, T.-W.; Gray, S. K. *Phys. Rev. B* **2005**, *71*, No. 035423.
(13) Sukharev, M.; Seideman, T. *Nano Lett.* **2006**, *6*, 715–719.
(14) Reuter, M. G.; Sukharev, M.; Seideman, T. *Phys. Rev. Lett.* **2008**, *101*, 208303.
(15) Taflove, A.; Hagness, S. C. *Computational Electrodynamics: The Finite-Difference Time-Domain Method*, 3rd Ed.; Artech House: Norwood, MA, 2005.
(16) Montgomery, J. M.; Lee, T.-W.; Gray, S. K. *J. Phys.: Condens. Matter* **2008**, *20*, 323201.
(17) Lee, T.-W.; Gray, S. K. *Opt. Express* **2005**, *13*, 9652–9659.
(18) Johnson, B. P.; Christy, R. W. *Phys. Rev. B* **1972**, *6*, 4370–4379.
(19) Liu, M.; Lee, T.-W.; Gray, S. K.; Guyot-Sinnest, P.; Pelton, M. *Phys. Rev. Lett.* **2009**, *102*, 107401.
(20) Chowdhury, M. H.; Pond, J.; Gray, S. K.; Lakowicz, J. R. *J. Phys. Chem. C* **2008**, *112*, 11236–11249.
(21) Tannor, D. J. *Introduction to Quantum Mechanics A Time-Dependent Perspective*; University Science Books: Sausalito, CA, 2007.
(22) Backus, S.; Durfee, C. G.; Murnane, N. N.; Kapteyn, *Rev. Sci. Instrum.* **1998**, *69*, 1207.
(23) Krause, J. L.; Whitnell, R. M.; Wilson, K. R.; Yan, Y. *J. Chem. Phys.* **1993**, *99*, 6562.
(24) Liau, Y.; Unterreiner, A.; Chang, Q.; Scherer, N. F. *J. Phys. Chem. B* **2001**, *105*, 2135–2142.
(25) Bisio, F.; Nyvlt, M.; Franta, J.; Petek, H.; Kirschner, J. *Phys. Rev. Lett.* **2006**, *96*, No. 087601.
(26) Feldstein, M. J.; Vöhringer, P.; Wang, W.; Scherer, N. F.; *J. Phys. Chem.* **1996**, *100*, 4739–4748.
(27) Liau, Y.-H.; Feldstein, M.; Scherer, N. F. *Ultrafast Phenom. XI* **1998**, *63*, 156–158.

DOI: 10.1021/nl101285t | *Nano Lett.* **2010,** *10,* 3389–3394